arXiv:1206.3427v1 [cond-mat.supr-con] 15 Jun 2012

Kinks and waterfalls as signatures of competing order in angle-resolved photoemission spectra of $La_{2-x}Sr_xCuO_4$

G. Mazza[1,2], M. Grilli[2,3], C. Di Castro[2,3], and S. Caprara[2,3]
[1] *International School for Advanced Studies (SISSA), Via Bonomea 265 34136 Trieste, Italy*
[2] *CNISM and Dipartimento di Fisica, Università di Roma "La Sapienza" Piazzale Aldo Moro 5, I-00185 Roma, Italy*
[3] *Consiglio Nazionale delle Ricerche, Istituto dei Sistemi Complessi, via dei Taurini, I-00185 Roma, Italy*

We show that the so-called *kinks* and *waterfalls* observed in angle-resolved photoemission spectra of $La_{2-x}Sr_xCuO_4$, a prototypical high-T_c superconducting cuprate, result from the coupling of quasiparticles with *two* distinct nearly critical collective modes with finite characteristic wave vectors, typical of charge and spin fluctuations near a stripe instability. Both phonon-like charge and spin collective modes are needed to account for the kinked quasiparticle dispersions. This clarifies the long-standing question whether kinks are due to phonons or spin waves and the nature of the bosonic mediators of the electron-electron effective interaction in $La_{2-x}Sr_xCuO_4$.

The metallic phase of high-T_c superconducting cuprates evolves remarkably with changing the temperature T and the doping x. A normal Fermi-liquid behavior is only found in overdoped samples, with x larger than the optimal value $x_{\rm opt}$ (where the maximum superconducting critical temperature T_c is achieved). At $x \approx x_{\rm opt}$ and $T > T_c$ the metallic phase seems to be ruled by the temperature as the only relevant energy scale, a typical signature of quantum criticality. In underdoped samples, with $x < x_{\rm opt}$, an even stronger anomaly is found, with a pseudogap opening around the Fermi energy, below a doping dependent temperature $T^*(x)$. Whether this is accompanied by the onset of some sort of ordering is still matter of debate. Nonetheless, models with nearly critical collective modes (CMs) coupled to fermion quasiparticles (QPs) may not only explain the anomalous metallic phase, but also provide candidate mediators of a retarded pairing interaction (the so-called *glue*) [1–3], alternative to phonons in ordinary superconductors, and are therefore actively investigated. Various proposals for sources of nearly critical CMs include the antiferromagnetic phase at $x \approx 0$ [4], time-reversal-breaking plaquette currents [5], order parameters with exotic wave symmetry [6, 7], or stripe ordering [8, 9].

In this Letter, we show that the so-called *kinks* and *waterfalls* [10] observed in angle-resolved photoemission spectroscopy (ARPES) identify charge (C) and spin (S) CMs on the verge of a stripe instability as the main source of scattering in $La_{2-x}Sr_xCuO_4$ (LSCO), solving the long-standing phonon-vs-spin issue, at least in LSCO. The sudden changes in the QP velocity (kinks) occurring at different energies in different regions of the Brillouin Zone (BZ), have often been attributed to a phonon with a near frequency [11, 12], and it has been argued that S fluctuations could account for the kinks in $YBa_2Cu_3O_{7-x}$ (YBCO) [13], and $Bi_2Sr_2CaCu_2O_8$ (BSCCO) [14]. We show that the same CMs also account for the sudden, nearly vertical, drops of the QP dispersions at high/moderate binding energies (waterfalls) [15, 16].

A previous survey of Raman spectra [17] for $x = 0.15 - 0.26$ and various T provided evidence for *two* distinct CMs peaked at finite characteristic wave vectors in LSCO [18]. One CM, essentially propagating and centered at typical phonon frequencies, is associated with C fluctuations (strongly mixed with the lattice degrees of freedom) near an incommensurate charge-density wave instability. The other CM, more diffusive and extending to higher energies, is associated with S fluctuations peaked near the wave vector of antiferromagnetic order. The behavior of the characteristic low-energy scale of the two CMs suggests that a quantum critical point occurs at $x_{QCP} \approx 0.19$ [21–23], associated to a phase with stripe-like C and S modulation, whose onset occurs via a harmonic incommensurate charge-density wave at $T \approx T^*(x)$ [9, 24, 25]. Remarkably, the strengths of the two CMs have an opposite x dependence (see Fig. 5 in Ref. [17]): The strength of the S CM decreases with increasing x and almost vanishes in the most overdoped sample ($x = 0.26$), whereas the strength of the C CM increases with increasing x and tends to saturate in the overdoped regime. The value $x \approx 0.19$ marks the boundary between the spin- and the charge-dominated region. At small x, S fluctuations are naturally enhanced by incipient antiferromagnetism, whereas in the optimally and overdoped regime C fluctuations dominate.

Here, we phenomenologically proceed to analyze the implications of the same two CMs, as derived from Raman experiments, on QP spectra. We consider the general Gaussian form of CM propagator

$$\mathcal{D}_\lambda(\mathbf{q},\omega_n) = -\frac{1}{\Upsilon_\lambda(\mathbf{q}-\mathbf{Q}_\lambda) + |\omega_n| + \omega_n^2/\overline{\Omega}_\lambda}, \quad (1)$$

where $\lambda = C, S$, ω_n is the bosonic Matsubara frequency, $\Upsilon_\lambda(\mathbf{q}) = m_\lambda + \nu_\lambda\,[2 - \cos(q_x a) - \cos(q_y a)]$ describes the dispersion of a lattice periodic CM, and reproduces the behavior $\Upsilon_\lambda(\mathbf{q}-\mathbf{Q}_\lambda \approx 0) \approx m_\lambda + \frac{1}{2}\nu_\lambda(\mathbf{q}-\mathbf{Q}_\lambda)^2$ obtained in different contextes for C [9] and S [4, 26] CMs. m_λ is proportional to the inverse squared correlation length ξ_λ^{-2}, ν_λ sets the curvature at the bottom of the CM dispersion law, and a is the spacing of the two-dimensional square lattice describing the CuO_2 planes of cuprates,

henceforth taken as unit length. The propagator (1) is peaked at a characteristic wave vector $\mathbf{Q}_\lambda$, has a diffusive character at low energy, and becomes more propagating above the energy scale $\overline{\Omega}_\lambda$. The CM dispersion is limited by an energy cutoff Λ_λ, setting a momentum cutoff $|\overline{\mathbf{q}}_\lambda| \approx (\Lambda_\lambda/\nu_\lambda)^{1/2}$. The values of the characteristic wave vectors, $\mathbf{Q}_C$ and $\mathbf{Q}_S$, are extracted from neutron scattering experiments: The incommensurability of the S density modulation, half of the incommensurability of the C density modulation when observed at $x = 1/8$ [30, 31], saturates for $x > 1/8$, yielding [32] $\mathbf{Q}_C = \pi\left(\pm\frac{1}{2}, 0\right), \pi\left(0, \pm\frac{1}{2}\right)$, $\mathbf{Q}_S = \pi\left(1 \pm \frac{1}{4}, 1\right), \pi\left(1, 1 \pm \frac{1}{4}\right)$.

We adopt for the fermion QPs on the CuO_2 planes of LSCO a tight-binding dispersion law including nearest ($t = 400$ meV) and next-to-nearest ($t' = -0.21t$) neighbor hopping terms,

$$\epsilon_{\mathbf{k}} = -2t\left(\cos k_x + \cos k_y\right) - 4t' \cos k_x \cos k_y - \mu, \quad (2)$$

where μ is the chemical potential. Similarly to the electron-phonon coupling, QPs are here coupled to CMs through dimensional coupling constants g_λ. The survey of Raman data on LSCO [17] yielded the doping evolutions of m, Λ, $\overline{\Omega}$, and $\kappa \equiv g^2/t\nu$, reported in Tab. I. Our aim is to fit ARPES data with the *same* CM parameters, although it should be borne in mind that Raman response is a momentum integrated quantity, so that the precise $\mathbf{q}$ dependence of the CM-mediated effective interaction, and therefore the value of $\overline{\mathbf{q}}$, is not fully constrained. We adjust $\overline{\mathbf{q}}$ as a fitting parameter [27], which in turn fixes $\nu = \Lambda/\overline{\mathbf{q}}^2$ and $g = \sqrt{\kappa t \nu}$. The obtained values (see Tab. I), yield four peaks in the CM dispersion, consistent with the observation of four separate peaks for the S CM in neutron scattering experiments [30, 32].

The effect of CMs on QP spectra is captured computing the lowest-order QP self-energy $\Sigma(\mathbf{k},\omega) = \Sigma_C(\mathbf{k},\omega) + \Sigma_S(\mathbf{k},\omega)$, and the single-particle spectral density

$$A(\mathbf{k},\omega) = \frac{1}{\pi} \frac{|\mathrm{Im}\Sigma(\mathbf{k},\omega)|}{\left[\omega - \epsilon_{\mathbf{k}} - \mathrm{Re}\Sigma(\mathbf{k},\omega)\right]^2 + \left[\mathrm{Im}\Sigma(\mathbf{k},\omega)\right]^2}.$$

The imaginary part of the self-energy is

$$\mathrm{Im}\Sigma_\lambda(\mathbf{k},\omega) = g_\lambda^2 \int_{BZ} \frac{d^2\mathbf{q}}{(2\pi)^2}\, \gamma_{\mathcal{Q}_\lambda}(\mathbf{q} - \mathbf{Q}_\lambda) \times \frac{(\omega - \epsilon_{\mathbf{k}-\mathbf{q}})\left[f_+(\epsilon_{\mathbf{k}-\mathbf{q}}) + f_-(\epsilon_{\mathbf{k}-\mathbf{q}} - \omega)\right]}{\left[\Upsilon_\lambda(\mathbf{q} - \mathbf{Q}_\lambda) - (\omega - \epsilon_{\mathbf{k}-\mathbf{q}})^2/\overline{\Omega}_\lambda\right]^2 + (\omega - \epsilon_{\mathbf{k}-\mathbf{q}})^2}, \quad (3)$$

where a sum over the star of equivalent wave vectors $\mathbf{Q}_\lambda$ is understood, $f_\pm(\omega) = 1/\left(e^{\omega/T} \pm 1\right)$, and the smooth cutoff function $\gamma_{\mathcal{Q}}(\mathbf{q}) = \exp\left[-\left(2 - \cos q_x - \cos q_y\right)/\mathcal{Q}^2\right]$ accounts for the suppression of the CM-QP coupling away from $\mathbf{Q}_\lambda$. As an order-of-magnitude estimate, $\mathcal{Q}_\lambda \approx |\overline{\mathbf{q}}_\lambda|$. For any given $\mathbf{k}$ and ω, we numerically integrate Eq. (3) and obtain $\mathrm{Re}\Sigma$ via Kramers-Kronig transformation. The chemical potential μ is fixed imposing that

$$2\int_{BZ} \frac{d^2\mathbf{k}}{(2\pi)^2} \int_{-\infty}^{+\infty} d\omega\, A(\mathbf{k},\omega) f_+(\omega) = 1 - x.$$

Charge

x	m (meV)	Λ (meV)	$\overline{\Omega}$ (meV)	κ	$\overline{\mathbf{q}}$	ν (meV)	$\mathcal{Q}$
0.15	2.5	248.0	25.0	5.5	0.9	300.0	0.6
0.17	4.35	248.0	25.0	8.0	0.9	300.0	0.6
0.20	8.7	310.0	25.0	11.7	1.0	300.0	0.5
0.25	9.9	186.0	41.3	13.7	0.9	240.0	0.5
0.26	7.55	300.0	41.3	17.5	1.0	280.0	0.55

Spin

x	m (meV)	Λ (meV)	$\overline{\Omega}$ (meV)	κ	$\overline{\mathbf{q}}$	ν (meV)	$\mathcal{Q}$
0.15	0.62	86.8	248.0	4.35	0.57	260.0	0.75
0.17	0.62	74.4	310.0	4.5	0.6	200.0	0.6
0.20	0.74	86.8	496.0	1.4	0.57	270.0	0.95
0.25	1.25	62.0	496.0	0.26	0.5	240.0	1.0
0.26	1.5	49.6	155.0	0.40	0.42	280.0	0.85

TABLE I. Parameters of the C and S CMs: m, Λ, $\overline{\Omega}$, and κ are extracted from Raman data [17].

We calculate the ARPES intensity convoluting $A(\mathbf{k},\omega)$ with a Gaussian of width ≈ 10 meV, mimicking energy resolution, and considering only the occupied states.

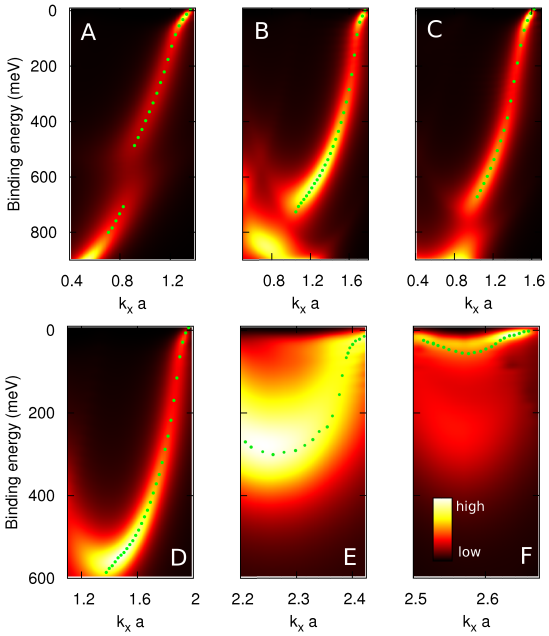

FIG. 1. (Color online) Spectral density along the cuts of the BZ reported in Fig. 2, for $x = 0.15$ and $T = 40$ K. Dots represent the maxima of the MDCs.

The main features of ARPES data are determined by the dynamical structure of the CMs of Eq. (1). In Fig. 1, we report the spectra along the cuts A-F of Fig. 2, for $x = 0.15$ and $T = 40$ K. We track the QP disper-

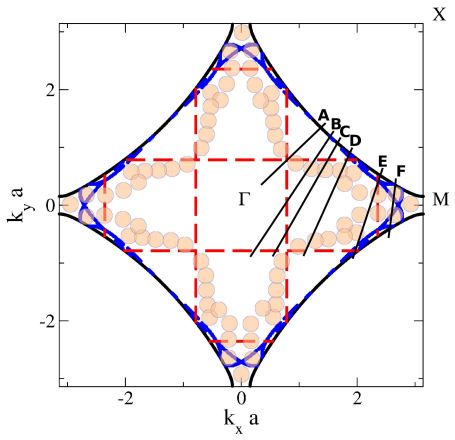

FIG. 2. (Color online) Fermi surface of LSCO at $x = 0.15$ (black solid line). The dashed (red online) and solid (blue online) lines mark the C and S hot lines, respectively. The shaded circles mark the loci of the waterfalls (from Ref. [16]). The spectra in Figs. 1,3 are calculated along the cuts A-F.

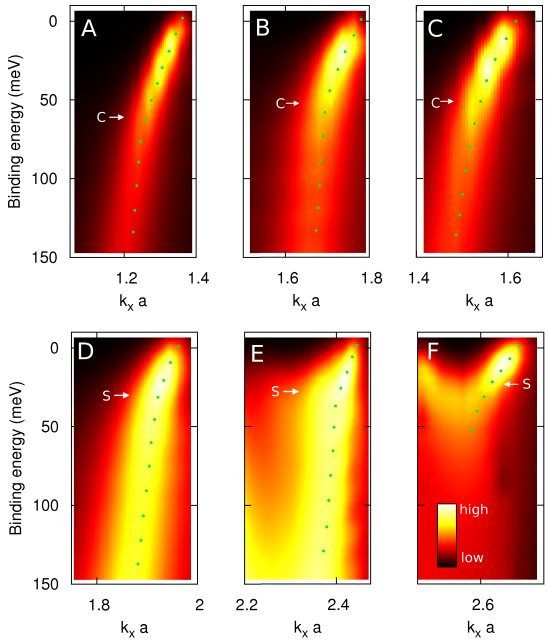

FIG. 3. (Color online) Same as in Fig. 1, but on a narrower energy range. Although the structure of the kinks is due to both S and C CMs, the arrows mark the kinks due to (mostly) C or S scattering.

sions (dots) as the maxima of the momentum distribution curves (MDCs). The condition of quasi criticality (small m_λ) and the finite values of the characteristic wave vectors $\mathbf{Q}_\lambda$ render the scattering most relevant when the QP momenta $\mathbf{k}$ satisfy the *hot line* condition $\epsilon_{\mathbf{k}} = \epsilon_{\mathbf{k}\pm\mathbf{Q}_\lambda}$, identifying the points at the same energy on the QP bands, connected by the characteristic wave vectors. We report in Fig. 2 the hot lines for C [(red) dashed lines] and S [(blue) solid lines] CMs. These lines intersect the Fermi surface at the so-called *hot spots*. Away from the hot lines, the scattering in Eq. 3 is not dominated by the nearly critical (low-energy) CM spectrum, and is rather mediated by the whole dynamical range of the order of $\sqrt{\overline{\Omega}\Lambda}$ [27]. This determines the energy scale of the kinks appearing at low binding energy ($\lesssim 70\,$meV) in Fig. 1. The strong scattering near the hot lines, reminiscent of the Bragg scattering occurring when some ordering takes place at specific $\mathbf{Q}_\lambda$, gives instead rise to the high-energy waterfall features in Fig. 1 [33].

We obtain waterfalls that compare fairly well with the experiments [10, 15, 16], although our perturbative scheme underestimates their binding energy and broadening. In particular, our hot lines reproduce the loci of the BZ where the waterfalls are observed [16] (shaded circles in Fig. 2). The waterfalls along the cuts A-C (at binding energies $\approx 600\,$meV, $\approx 300\,$meV, and $\approx 250\,$meV, respectively) correspond to the nearly cross-shaped accumulation of the loci well inside the BZ in Fig. 2. In our scheme, these are due to C incipient order, which also produces additional waterfalls along a square contour surrounding the Γ point of the BZ. These are visible in panels B and C of Fig. 1, at approximately $700 - 800\,$meV. Their presence cannot be ascertained in Ref. [16], where the data at higher binding energy are not reported. A reanalysis of the data is required to check for the presence of these additional waterfalls.

On the other, hand both the C and S scattering are responsible for the dense occurrence of waterfalls near the M points (cuts D-F in Fig. 2). However, as it is clear from panels D-F in Fig. 1, the waterfalls are shifted to lower binding energy in this region of the BZ and merge with the kinks. Morover, approaching the hot spots, the waterfall evolves into a rounding of the QP dispersions, with a spectral intensity vanishing as $\sqrt{\omega}$ [4, 34, 35]. This rounding is reminiscent of the additional low-energy kinks observed in BSCCO [36, 37], but not in LSCO, possibly due to a lower resolution.

To follow the evolution of the kinks, we show in Fig. 3 the low-energy spectra, along the same cuts of Fig. 1. In the nodal (ΓX) direction (cut A), the waterfall is well separated from the low-energy kink, which is more closely inspected in Fig. 4 (a). Here we report the kinked dispersion separately due to C [(red) squares] and S [(green) diamonds] CMs, and to the combination of both [(blue) circles]. The binding energy of the kink [(blu) arrow in Fig. 4 (a)] is clearly set by the C CM [(red) arrow], at $\approx 60 - 70\,$meV, in good agreement with the experimental dispersion for LSCO at the same doping and temperature [38]. The markedly propagating character of the C CM (phonon-like away from the hot lines [27, 28, 35]) makes its contribution to the kink rather sharp.

We emphasize that the characteristic energy of the C CM is extracted from Raman experiments (Tab. I) and

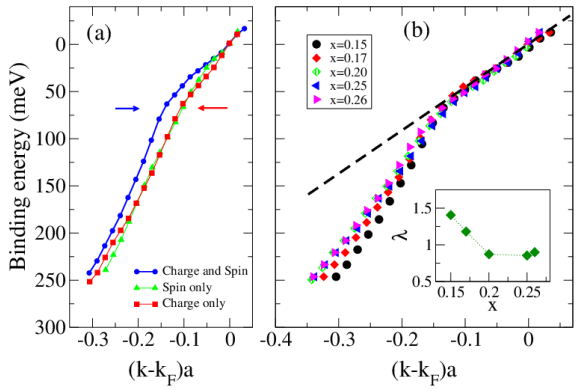

FIG. 4. (Color online) (a) QP dispersion along the ΓX direction for LSCO at $x = 0.15$ and $T = 40$ K in the presence of both C and S CMs (solid circles, blue online) and for C (squares, red online) or S (triangles, green online) only. (b) Doping evolution of the kink. Both C and S CMs are considered, and $T = 40$ K. The dashed straight lines marks the low-energy dispersion. Inset: doping evolution of $\lambda \equiv (v_{HE}/v_F) - 1$ (see text).

is not adjusted here by introducing additional modes at suitably chosen phonon frequencies. On the other hand, the more diffusive S CM does not fix an energy scale and rather renormalizes the bare QP dispersion over a broader energy range, affecting the QP velocities far from the kink and making the kink more pronounced. Both C and S CMs must be simultaneously taken into account in order to quantitatively explain the kink. The analysis of Raman spectra shows that the interaction mechanism switches from S to C CM with increasing x [17]. This characterizes the doping evolution of the QP dispersion in the range $x = 0.15 - 0.26$ [38]. In Fig. 4 (b), one sees that the S-vs-C switching produces no appreciable effect on the low-energy dispersion, which is determined cooperatively by the two CMs, so that the slope remains quite constant in the doping considered range [dashed line in Fig. 4 (b)]. On the other hand, in the high-energy dispersion, where most of the effect of the C CM is exhausted and the variation of the slope is controlled by the the S CM, the dispersion becomes less steep with increasing doping, so that the high-energy QP velocity decreases. This is clearly observed looking at the inset in Fig. 4 (b), where the parameter $\lambda \equiv (v_{HE}/v_F) - 1$, measuring the strength of the (mostly S-mediated) interaction, is plotted vs. x. Although our analysis was limited to $x \geq 0.15$, extrapolating to the underdoped region the increasing strength of the S-mediated scattering (see Ref. [17]), we can also account for the observed [38] increase of the parameter λ (mainly due to the increase of v_{HE}) below $x = 0.15$.

Along different cuts in the BZ, the QP dispersion is differently affected by the two CMs, which may yield kinks (see Fig. 3) at energies depending on the CM dispersion and on the position of the cut with respect to the hot lines. The kink due to the C CM moves to lower energies when the cut moves to the region where the C hot line approaches the Fermi surface (cuts B and C). On the other hand, the S hot lines track rather closely the Fermi surface, giving rise to the above mentioned rounding of the dispersion at very low energy ($\lesssim 20$ meV). Along the cuts D-F, the C and S hot lines have intricate structures, which makes it difficult to distinguish the role of the two CMs in determining the mixed kink-waterfall structures. Nonetheless, by switching on and off the C and S couplings, we can state that the S CM plays the major role in this region of the BZ.

The C-S cooperative behavior might be specific of LSCO, where the tendency to charge ordering seems to be more pronounced than, e.g., in YBCO, where the kinks are more rounded. We also stress that our analysis only holds above T_c. Below T_c the S CM changes and displays the peculiar resonance at (π, π), which alters the shape of the kinks, producing a characteristic s-shaped dispersion in the antinodal regions [14, 39]. On the other hand, the rather broad and moderately coupled phonons should keep their effects (most pronounced around the nodal regions) even in the superconducting phase.

In conclusion, the salient aspects of ARPES experiments in LSCO are well reproduced by the *same* two (C and S) CMs previously obtained to fit Raman experiments. This solves for LSCO the long-standing issue whether the kinks are due to phonons or spin fluctuations: we reach the Solomonic conclusion that both play a role. By the interplay of the two CMs, we can explain the highly non-trivial doping evolution of the low- and high-energy QP velocity along the nodal (ΓX) direction, with v_F almost doping independent and v_{HE} decreasing with increasing doping (along with the suppression of the coupling with the S CM). We predict the presence of multiple kinks (actually, a kink and a low-energy rounding, analogous to those observed in BSCCO [36, 37]). We also predict additional waterfalls at high binding energy, along a square contour around the Γ point of the BZ.

Since, our analysis demonstrates the presence of *two* CMs, with characteristic wave vectors representative of stripe-like textures, our phenomenological model substantiates the presence of a competing C and S quasi-ordered phase compatible with fluctuating stripes. The assessed relevant role of C and S CMs in LSCO also identifies them as candidate mediators of the pairing glue in these systems.

S.C., C. D.C., and M.G. acknowledge financial support from "University Research Project" of the "Sapienza" University n. C26A115HTN.

[1] P. W. Anderson, Science **316**, 1705 (2007).

[2] T. A. Maier, D. Poilblanc, and D. J. Scalapino, Phys. Rev. Lett. **100**, 237001 (2008).

[3] W. Hanke, M. L. Kiesel, M. Aichhorn, S. Brehm, and E. Arrigoni, Eur. Phys. J. Special Topics **188**, 15 (2010).

[4] Ar. Abanov, A. Chubukov, and J. Schmalian, Adv. Phys. **52**, 119 (2003), and references therein.

[5] C. M. Varma, Phys. Rev. Lett. 75, 898 (1995); Phys. Rev. B **55**, 14554 (1997), and references therein.

[6] L. Benfatto, S. Caprara, and C. Di Castro, Eur. Phys. J. B **17**, 95 (2000).

[7] W. Metzner, D. Rohe, and S. Andergassen, Phys. Rev. Lett. **91**, 066402 (2003).

[8] S. A. Kivelson, I. P. Bindloss, E. Fradkin, V. Oganesyan, J. M. Tranquada, A. Kapitulnik, and C. Howald, Rev. Mod. Phys. **75**, 1201 (2003) and references therein.

[9] C. Castellani, C. Di Castro, and M. Grilli, Phys. Rev. Lett. **75**, 4650 (1995).

[10] For a review, see, e.g., D. R. Garcia and A. Lanzara, Adv. Cond. Mat. Phys. Volume 2010, Article ID 807412, doi:10.1155/2010/807412, and references therein.

[11] P. V. Bogdanov, A. Lanzara, S. A. Kellar, X. J. Zhou, E. D. Lu, W. J. Zheng, G. Gu, J.-I. Shimoyama, K. Kishio, H. Ikeda, R. Yoshizaki, Z. Hussain, and Z. X. Shen, Phys. Rev. Lett. **85**, 2581 (2000).

[12] X. J. Zhou, T. Cuk, T. Devereaux, N. Nagaosa, and Z.-X. Shen, "Angle-Resolved Photoemission Spectroscopy on Electronic Structure and Electron-Phonon Coupling in Cuprate Superconductors", Handbook of High-Temperature Superconductivity: Theory and Experiment, edited by J. R. Schrieffer, (Springer, 2007), Pages 87-144.

[13] T. Dahm, V. Hinkov, S. V. Borisenko, A. A. Kordyuk, V. B. Zabolotnyy, J. Fink, B. Bchner, D. J. Scalapino, W. Hanke and B. Keimer, Nat. Phys. **5**, 217 (2009).

[14] A. V. Chubukov and M. R. Norman, Phys. Rev. B **70**, 174505 (2004).

[15] J. Graf, G.-H. Gweon, K. McElroy, S. Y. Zhou, C. Jozwiak, E. Rotenberg, A. Bill, T. Sasagawa, H. Eisaki, S. Uchida, H. Takagi, D.-H. Lee, and A. Lanzara, Phys. Rev. Lett. **98**, 067004 (2007).

[16] J. Chang, S. Pailhés, M. Shi, M. Mnsson, T. Claesson, O. Tjernberg, J. Voigt, V. Perez, L. Patthey, N. Momono, M. Oda, M. Ido, A. Schnyder, C. Mudry, and J. Mesot, Phys. Rev. B **75**, 224508 (2007).

[17] S. Caprara, C. Di Castro, B. Muschler, W. Prestel, R. Hackl, M. Lambacher, A. Erb, S. Komiya, Y. Ando, and M. Grilli, Phys. Rev. B **84** , 054508 (2011).

[18] The presence of two collective modes has also been inferred from optical and experiments in BSCCO systems in Refs. [19, 20]

[19] E. van Heumen, E. Muhlethaler, A. B. Kuzmenko, H. Eisaki, W. Meevasana, M. Greven, and D. van der Marel, Phys. Rev. B **79**, 184512 (2009).

[20] S. Dal Conte, C. Giannetti, G. Coslovich, F. Cilento, D. Bossini, T. Abebaw, F. Banfi, G. Ferrini, H. Eisaki, M. Greven, A. Damascelli, D. van der Marel, F. Parmigiani, Science **335**, 1600 (2012)

[21] C. Castellani, C. Di Castro, and M. Grilli, Z. Phys. B **103**, 137144 (1997).

[22] C. Castellani, C. Di Castro, and M. Grilli, J. Phys. Chem. Solids **59**, 1694 (1998).

[23] J. L. Tallon and J. W. Loram, Physica C **349**, 53 (2001).

[24] A. Perali, C. Castellani, C. Di Castro, and M. Grilli, Phys. Rev. B **54**, 16216 (1996).

[25] S. Andergassen, S. Caprara, C. Di Castro, and M. Grilli, Phys. Rev. Lett. **87**, 056401 (2001).

[26] A. J. Millis, H. Monien, and D. Pines, Phys. Rev. B **42**, 167 (1990).

[27] Microscopic calculations [28] show that the C CM essentially has a flattish phononic dispersion $\sim \omega_0$, which, near the C instability, is substantially softened in a limited momentum region around $\mathbf{Q}_C$. The parameter $\overline{\mathbf{q}}_C$ sets the width of this region, where a parabolic dispersion in the poles of Eq. (1) extends from the energy scale m_C, to $\sqrt{\overline{\Omega}_C \Lambda_C}$. We assume that a similar momentum cutoff is present for the S CM. One can also show [29] that $\overline{\Omega}_C \approx \omega_0^2/t$ and $\Lambda_C \approx t$, yielding $\sqrt{\overline{\Omega}_C \Lambda_C} \approx \omega_0$.

[28] F. Becca, M. Tarquini, M. Grilli, and C. Di Castro, Phys. Rev. B **54**, 12443 (1996).

[29] S. Caprara, M. Grilli, C. Di Castro, and T. Enss, Phys. Rev. B **75**, 140505(R) (2007).

[30] J. M. Tranquada, B. J. Sternlieb, J. D. Axe, Y. Nakamura, and S. Uchida, Nature (London) **375**, 561 (1995).

[31] P. Abbamonte, A. Rusydi, S. Smadici, G. D. Gu, G. A. Sawatzky, and D. L. Feng, Nat. Phys. **1**, 155 (2005).

[32] K. Yamada, C. H. Lee, K. Kurahashi, J. Wada, S. Wakimoto, S. Ueki, H. Kimura, Y. Endoh, S. Hosoya, G. Shirane, R. J. Birgeneau, M. Greven, M. A. Kastner, and Y. J. Kim, Phys. Rev. B **57**, 6165 (1998).

[33] An explanation of the waterfalls observed in BSCCO in terms of an electronic (spin) generated self-energy was proposed by Susmita Basak, Tanmoy Das, Hsin Lin, J. Nieminen, M. Lindroos, R. S. Markiewicz, and A. Bansil, Phys. Rev. B **80**, 214520 (2009). In this case, however, only one (spin) mode was considered and the momenta where the waterfalls occur were not reported.

[34] A. V. Chubukov, D. K. Morr, and A. Shakhnovich, Philos. Mag. B **74**, 563 (1996); A. V. Chubukov and D. K. Morr, Phys. Rep. **288**, 347 (1998).

[35] S. Caprara, M. Sulpizi, A. Bianconi, C. Di Castro, and M. Grilli, Phys. Rev. B **59**, 14980 (1999).

[36] I. M. Vishik, W. S. Lee, F. Schmitt, B. Moritz, T. Sasagawa, S. Uchida, K. Fujita, S. Ishida, C. Zhang, T. P. Devereaux, and Z. X. Shen, Phys. Rev. Lett. **104**, 207002 (2010)

[37] S. Johnston, I. M. Vishik, W. S. Lee, F. Schmitt, S. Uchida, K. Fujita, S. Ishida, N. Nagaosa, Z. X. Shen, and T. P. Devereaux, Phys. Rev. Lett. **108**, 166404 (2012).

[38] S. Sahrakorpi, R. S. Markiewicz, Hsin Lin, M. Lindroos, X. J. Zhou, T. Yoshida, W. L. Yang, T. Kakeshita, H. Eisaki, S. Uchida, Seiki Komiya, Yoichi Ando, F. Zhou, Z. X. Zhao, T. Sasagawa, A. Fujimori, Z. Hussain, Z.-X. Shen, and A. Bansil, Phys. Rev. B **78**, 104513 (2008).

[39] U. Chatterjee, D. K. Morr, M. R. Norman, M. Randeria, A. Kanigel, M. Shi, E. Rossi, A. Kaminski, H. M. Fretwell, S. Rosenkranz, K. Kadowaki, and J. C. Campuzano, Phys. Rev. B **75**, 172504 (2007).